

Conductivity of Dirac fermions with phonon induced topological crossover

Zhou Li^{1*} and J. P. Carbotte^{1,2}

¹ *Department of Physics, McMaster University, Hamilton, Ontario, Canada L8S 4M1*

² *Canadian Institute for Advanced Research, Toronto, Ontario, Canada M5G 1Z8*

(Dated: June 18, 2021)

We study the Hall conductivity in single layer gapped Dirac fermion materials including coupling to a phonon field, which not only modifies the quasi-particle dynamics through the usual self-energy term but also renormalizes directly the gap. Consequently the Berry curvature is modified. As the temperature is increased the sign of the renormalized gap can change and the material can cross over from a band insulator to a topological insulator at higher temperature (T). The effective Chern numbers defined for valley and spin Hall conductivity show a rich phase diagram with increasing temperature. While the spin and valley DC Hall conductivity is no longer quantized at elevated temperature a change in sign with increasing T is a clear indication of a topological crossover. The chirality of the circularly polarized light which is dominantly absorbed by a particular valley can change with temperature as a result of a topological crossover.

PACS numbers: 78.67.-n, 71.38.-k, 73.25.+i

I. INTRODUCTION

The isolation of graphene by exfoliation^{1,2} led to the discovery of many of its exotic properties^{3,4}. It also led to the fabrication and study of other two dimensional systems such as single layer group-VI dichalcogenides⁵⁻⁸ (e.g. MoS_2) and silicene⁹⁻¹¹, a buckled honeycomb lattice of silicon atoms. The Kane-Mele¹² low energy Hamiltonian can be used to describe these materials which have Dirac cones and valley degeneracy. The Dirac fermions can acquire mass and spin-orbit coupling can spin polarize the bands. Manipulation of the size of the gaps involved can lead to a topological phase transition from a quantum spin Hall state to a band insulator. It is known from consideration of the selection rules^{13,14} for the optical transition involving circularly polarized light that the two valleys with indices $\tau = \pm 1$ react oppositely to the incident photon. Each valley has opposite sign of orbital magnetic moment and Berry curvature, and right (left) handed polarized radiation excites preferentially valley $\tau = +1(-1)$. These materials display a rich phase diagram with phases having different topological quantum numbers (Chern numbers) and are believed to be ideal for valleytronics¹⁵⁻¹⁷.

Here we go beyond a bare band model and include in the Hamiltonian the coupling of the charge carriers to a phonon field¹⁸⁻²¹. We find that the spin and valley dependent gap is renormalized by the phonons and that this renormalization depends strongly on temperature²². Consequently the Berry curvature will be modified and the topological quantum numbers are not well protected. For example, as we increase temperature, the gap can close and reopen and as found by Garate²² the system can crossover from a band to a topological insulator. While reference [22] was concerned only with a proof in principle, here we show how this crossover can be measured experimentally either using spin and/or valley DC Hall conductivity or through the circular dichroism of absorbed light. The Kane-Mele model Hamiltonian is

specified in section II along with electron-phonon coupling based on the Holstein model. The self energy due to electron-phonon interaction directly modifies the gap which changes sign with increasing temperature (T). Formulas for AC longitudinal and transverse optical conductivity including self energy effects are presented in section III. The change in sign of the renormalized gap with increasing T can be viewed as changing the underlying Chern number and we describe a pathway to determining this topological crossover through DC valley and spin Hall effects. Section IV deals with the temperature dependence of the dichroism of circularly polarized light with the handedness of the dominant absorption changing sign with increasing temperature. Section V provides a brief conclusion.

II. FORMALISM AND RENORMALIZED GAP

The Kane-Mele model Hamiltonian¹² for gapped Dirac fermions with spin-orbit coupling takes the form

$$\hat{H}_0 = \hbar v(\tau k_x \hat{\sigma}_x + k_y \hat{\sigma}_y) + \Delta_z \hat{\sigma}_z - \lambda_{SO} \tau \hat{\sigma}_z \hat{S}_z, \quad (1)$$

where the valley index $\tau = \pm 1$, λ_{SO} is the spin orbit coupling parameter, Δ_z a gap and v is the Fermi velocity. For definiteness in our calculations we will use $\lambda_{SO} = 4meV$ and $v \approx 5 \times 10^5 m/s$ ⁹⁻¹¹. The $\hat{\sigma}'_s$ are the Pauli matrices for pseudospin and \hat{S}_z is the spin matrix for its z-component (s_z). Here we define the spin and valley dependent gap as $\Delta_{s_z}^\tau = \Delta_z - \lambda_{SO} \tau s_z$.

The Holstein electron-phonon interaction which has been widely used, is written as

$$H_{e-ph} = -g\omega_E \sum_{\mathbf{k}, \mathbf{k}', s} c_{\mathbf{k}, s}^\dagger c_{\mathbf{k}', s} (b_{\mathbf{k}' - \mathbf{k}}^\dagger + b_{\mathbf{k} - \mathbf{k}'}) + \sum_{\mathbf{q}} \omega_E b_{\mathbf{q}}^\dagger b_{\mathbf{q}}, \quad (2)$$

where $b_{\mathbf{q}}^\dagger$ creates a phonon of energy ω_E and momentum \mathbf{q} , g is a coupling between electrons and phonons and $c_{\mathbf{k}, s}^\dagger$

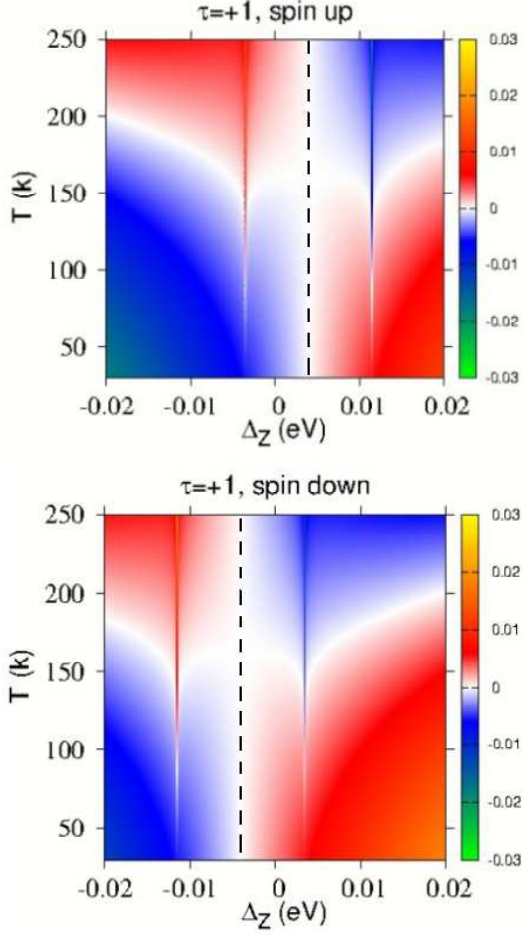


FIG. 1. (Color online) Temperature dependent renormalized gap $\hat{\Delta}_{s_z}^\tau$ for spin up (top frame) and spin down (bottom frame) charge carriers, as a function of the bare mass gap Δ_z . The vertical black dashed line indicate the line $\hat{\Delta}_{s_z}^\tau = \Delta_{s_z}^\tau = \text{Re}\Sigma^Z(\tau, s_z, 0) = 0$.

creates an electron of momentum \mathbf{k} and spin s . The self energy is given by¹⁸

$$\hat{\Sigma}(i\omega_n) = \Sigma^I(i\omega_n)\hat{I} + \Sigma^Z(i\omega_n)\hat{\sigma}_z \quad (3)$$

We are interested in the case when the chemical potential $\mu = 0$, so that μ lies in the gap. In this case the self energy $\text{Re}\Sigma^I(0) = 0$ so the chemical potential will not be shifted by the electron-phonon interaction. However $\Sigma^Z(i\omega_n \rightarrow \omega + i0^+)$ will modify the gap $\Delta_{s_z}^\tau$ at $\omega = 0$ and consequently the Berry curvature. We give an analytical expression here for the $\omega = 0$ limit

$$\text{Re}\Sigma^Z(\tau, s_z, 0) = \frac{g^2\omega_E^2\Delta_{s_z}^\tau}{2t^2\pi} \times \left[\ln\left|\frac{\omega_E + |\Delta_{s_z}^\tau|}{\omega_E + \sqrt{x_{cut}}}\right| + \frac{\ln\left[|\Delta_{s_z}^\tau|^2 - \omega_E^2\right]/(x_{cut}^2 - \omega_E^2)}{\exp(\omega_E/(k_B T)) - 1} \right] \quad (4)$$

Here $\sqrt{x_{cut}} = \sqrt{\hbar^2 v^2 k_{\max}^2 + (\Delta_{s_z}^\tau)^2}$ and $\hbar v k_{\max} = 3.5eV$. The electron-phonon coupling g is chosen to

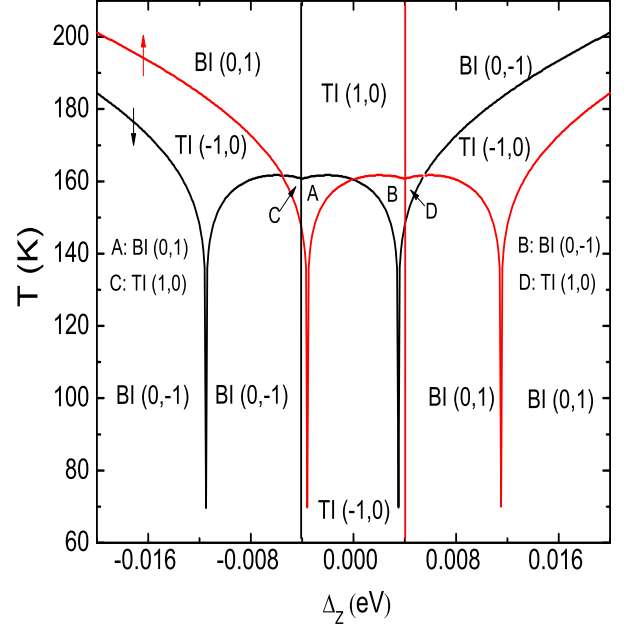


FIG. 2. (Color online) The phase diagram in the Δ_z - T plane. The red and black line (phase boundaries) indicate $\hat{\Delta}_{s_z}^\tau = 0$ for charge carriers in one valley with spin up and down respectively. The notation is BI (x,y) and TI (x,y) for band and topological insulator respectively with spin Chern number x and valley Chern number y. Increasing temperature can induce crossover from a band insulator to a topological insulator or vice versa.

make the effective mass correction to be about 0.2, which is a conservative estimate (a recent experiment in $\text{Cu}_x\text{Bi}_2\text{Se}_3$ ²³ found an order of magnitude larger effective mass than what we have used here) of a typical phonon coupling in semiconductors²⁴, ω_E is chosen to be $7.5meV$ and $t = \hbar v/a$ where a is the lattice constant, from this we know $t \approx 1.0eV$.

For this set of parameters the first term in Eq. (4) which gives the zero temperature value of the renormalization $\text{Re}\Sigma^Z(\tau, s_z, 0)$ provides a 22% correction to $\Delta_{s_z}^\tau$ which is small. The second term in Eq. (4) however can become large as temperature increases and $k_B T \gg \omega_E$. The interacting Green's function is given by

$$\hat{G}(\mathbf{k}, i\omega_n) = \frac{1}{2} \sum_{s=\pm} (1 + s\mathbf{H}_\mathbf{k} \cdot \boldsymbol{\sigma}) G(\mathbf{k}, s, i\omega_n) \quad (5)$$

with

$$\mathbf{H}_\mathbf{k} = \frac{(\hbar v \tau k_x, \hbar v k_y, \Delta_{s_z}^\tau + \Sigma^{Z*}(i\omega_n))}{\sqrt{\hbar^2 v^2 k^2 + |\Delta_{s_z}^\tau + \Sigma^Z(i\omega_n)|^2}} \quad (6)$$

and

$$G(\mathbf{k}, s, i\omega_n) = \frac{1}{i\omega_n + \mu - \lambda \tau s_z / 2 - E(\mathbf{k}, s, i\omega_n)} \quad (7)$$

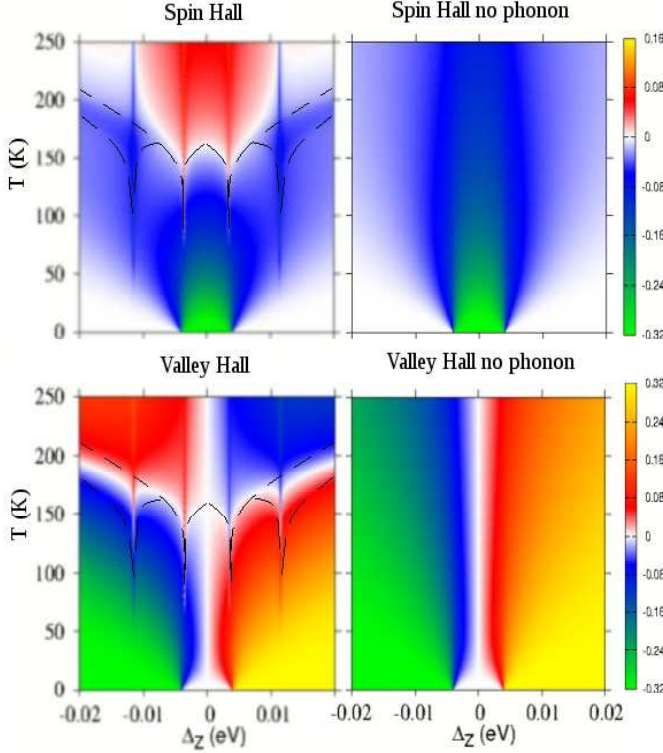


FIG. 3. (Color online) Color plot of the temperature dependent spin (top) and valley (bottom) Hall conductivity as a function of temperature T and mass gap Δ_z . Superimposed as long dashed black lines are the phase boundaries of Fig. 2.

where $E(\mathbf{k}, s, i\omega_n) = s\sqrt{[\Delta_{s_z}^\tau + \Sigma^z(i\omega_n)]^2 + \hbar^2 v^2 k^2} + \Sigma^I(i\omega_n)$. The self energy $\Sigma^I(i\omega_n)$ ¹⁹⁻²¹ directly renormalizes the quasiparticle energies when there is no gap ($\Delta_{s_z}^\tau = 0$). However when $\Delta_{s_z}^\tau$ is non zero we see that $\Sigma^Z(i\omega_n)$ enters Eq. (6) and Eq. (7) to directly renormalize the gap ($\Delta_{s_z}^\tau$). Thus the Berry curvature is renormalized by the electron-phonon interaction through the nontrivial gap self energy $\Sigma^Z(i\omega_n)$. At zero temperature, only the $\omega = 0$ limit of $\Sigma^Z(i\omega_n \rightarrow \omega + i0^+)$ enters the DC limit of the Hall conductivity which depends on the renormalized gap $\tilde{\Delta}_{s_z}^\tau = \Delta_{s_z}^\tau + Re\Sigma^Z(\tau, s_z, 0)$ and this plays a critical role in this work. In Fig. 1 we show a color plot of the magnitude of $\tilde{\Delta}_{s_z}^\tau$ as a function of the bare gap Δ_z and temperature T for fixed value of λ_{SO} . The top frame is for one valley, $\tau = +1$, and spin up, while the bottom frame is for spin down. The vertical dashed line at $\Delta_z = 4$ and $-4meV$ respectively indicates the line $\tilde{\Delta}_{s_z}^\tau = \Delta_{s_z}^\tau = Re\Sigma^Z(\tau, s_z, 0) = 0$. The renormalized gap has other zeros as indicated by the white curves which separate positive and negative regions of $\tilde{\Delta}_{s_z}^\tau$. This change in the sign of the gap indicate possible topological crossovers as we will discuss below.

III. FORMALISM AND AC LONGITUDINAL AND TRANSVERSE CONDUCTIVITY

The AC longitudinal conductivity $\sigma_{xx}(\omega)$ and transverse Hall conductivity $\sigma_{xy}(\omega)$ in the lowest order approximation, following from the Kubo formula without vertex corrections²⁵ are given by^{8,18}

$$\sigma_{xx}(\omega) = \frac{e^2}{\hbar^2} \int_{1,2} \sum_{\mathbf{k}} Tr \langle \sigma_x \hat{A}(\mathbf{k}, \omega_1) \sigma_x \hat{A}(\mathbf{k}, \omega_2) \rangle \quad (8)$$

where we are only interested in the absorptive part of the conductivity so no diamagnetic part is required²⁶,

$$\sigma_{xy}(\omega) = \frac{e^2}{\hbar^2} \int_{1,2} \sum_{\mathbf{k}} Tr \langle \tau_z \sigma_x \hat{A}(\mathbf{k}, \omega_1) \sigma_y \hat{A}(\mathbf{k}, \omega_2) \rangle \quad (9)$$

where $\hat{A}(\mathbf{k}, \omega)$ is the matrix spectral density, $\int_{1,2} = \int_{-\infty}^{\infty} d\omega_1 d\omega_2 F(\omega)$ and the function $F(\omega) = \frac{\hbar^2 v^2}{4\pi^2 i\omega} \frac{[f(\omega_1) - f(\omega_2)]}{\omega - \omega_2 + \omega_1 + i\delta}$. The optical conductivity for circularly polarized light follows as

$$Re\sigma_{\pm}(\omega) = Re\sigma_{xx}(\omega) \mp Im\sigma_{xy}(\omega) \quad (10)$$

Details on the impact of the self energies $\Sigma^I(i\omega_n)$ and $\Sigma^Z(i\omega_n)$ on the longitudinal and Hall optical conductivity are found in the reference¹⁸ to which the reader is referred.

We begin our discussion with the zero temperature DC limit of the spin and valley Hall conductivity, which can be associated to the spin and valley Chern numbers. Finite temperature will obscure this relationship, but we will still speak of an effective Chern number using the zero frequency renormalized gap calculated at finite T in the zero temperature bare band expressions for the conductivities. At finite temperature the Hall conductivity is then given by

$$Re\sigma_{xy} = \frac{e^2}{4\pi\hbar} \sum_{\tau, s_z} \tau \int k dk \frac{\hbar^2 v^2 \tilde{\Delta}_{s_z}^\tau [f(\varepsilon_{\mathbf{k}, -}) - f(\varepsilon_{\mathbf{k}, +})]}{[\tilde{\Delta}_{s_z}^\tau]^2 + \hbar^2 v^2 k^2]^{3/2}} \quad (11)$$

with $f(\omega)$ the Fermi-Dirac distribution function. For the spin and valley Hall conductivity τ in Eq. (11) should be replaced by $\hbar\tau s_z/(2e)$ and $1/e$ respectively. At $T = 0$ Eq. (11) reduces to

$$Re\sigma_{xy} = \frac{e^2}{4\pi\hbar} \sum_{\tau, s_z} \tau [sgn(\tilde{\Delta}_{s_z}^\tau)] \quad (12)$$

thus the spin and valley Hall conductivity remains quantized at $T=0$ in our treatment of the electron-phonon interaction. Its only effect is to change the value of $\tilde{\Delta}_{s_z}^\tau$ over its bare band value through the renormalization $Re\Sigma^Z(\tau, s_z, 0)$ of Eq. (4). The Chern number, spin Chern number and valley Chern number are defined as $C = \frac{1}{4} \sum_{\tau, s_z} \tau [sgn(\tilde{\Delta}_{s_z}^\tau)]$, $C_s = \frac{1}{4} \sum_{\tau, s_z} \tau s_z [sgn(\tilde{\Delta}_{s_z}^\tau)]$ and $C_v = \frac{1}{4} \sum_{\tau, s_z} [sgn(\tilde{\Delta}_{s_z}^\tau)]$. A phase diagram for the

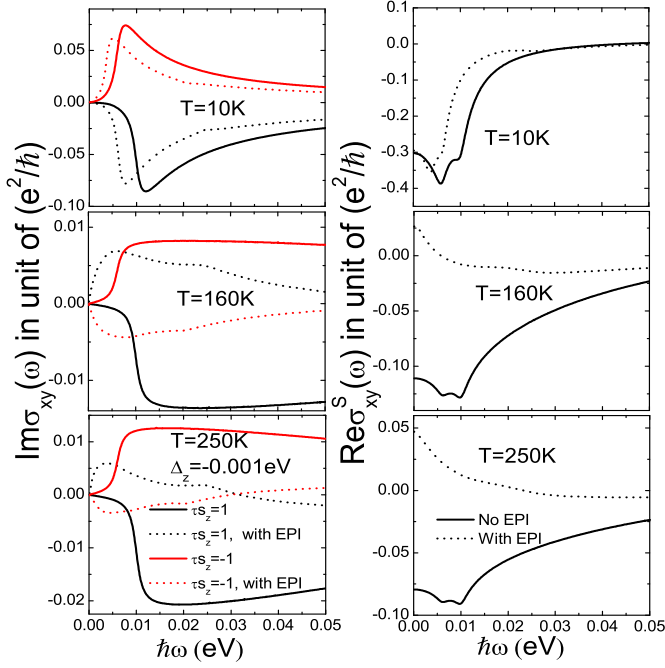


FIG. 4. (Color online) The real (right frames) and imaginary (left frames) of the transverse conductivity $\sigma_{xy}(\omega)$ in units of e^2/h vs. photon energy in eV for three temperatures $T = 10K, 160K$ and $250K$ from top to bottom. In all cases the gap $\Delta_z = 0.001eV$. Black lines are for $\tau s_z = 1$ and red for $\tau s_z = -1$. Solid curves are bare band results while dotted curves include the electron-phonon renormalizations and are based on Eq. (9).

effective Chern numbers obtained in this way is given in Fig. 2 with Δ_z on the horizontal axis and temperature T on the vertical axis. The solid black lines give the zeros of the renormalized gap $\tilde{\Delta}_{s_z}^r \equiv \Delta_{s_z}^r + Re\Sigma^Z(\tau, s_z, 0)$. The labels TI and BI indicate topological and band insulator respectively with right hand integer $0, \pm 1$ the effective valley Chern number and the left hand integer the effective spin Chern number. Once again we emphasize that these numbers are obtained from a $T = 0$ calculation for σ_{xy} of Eq. (12) using the value of the renormalized gap obtained at finite T . Of course for finite T one should really calculate the valley and spin Hall conductivity at the same T using the complete Eq. (9). Nevertheless Fig. 2 remains useful in defining the various regions involved and we will see that the phase boundaries defined in this figure remain imprinted in our finite T results although these boundaries are definitely fuzzed out by temperature. This is shown in Fig. 3 where we give a color plot of the spin and valley Hall DC conductivity obtained from the finite temperature formula Eq. (11). This equation is a simplification of Eq. (9) for the Hall conductivity. Eq. (9) includes the complete frequency dependent renormalization due to both $\Sigma^I(i\omega_n)$ and $\Sigma^Z(i\omega_n)$. The first accounts for the quasiparticle renormalizations which shifts the bare energies (real part)

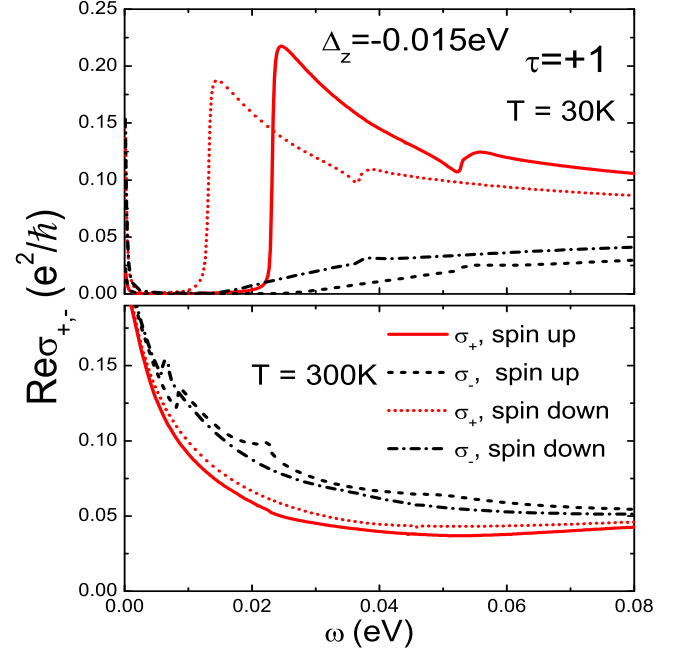


FIG. 5. (Color online) Temperature dependence of the dynamic optical conductivity of the circularly polarized light. The top frame is for $T = 30K$ (low temperature) and the bottom frame for $T = 300K$ (high temperature). The valley index is $\tau = 1$. Red lines are for right hand polarized light and the black for left hand. The contribution from spin up and spin down bands are given separately.

and provides damping (imaginary part). The second accounts for gap renormalization effects and also has frequency dependence and is complex. We have evaluated numerically this complete equation for a number of points in Fig. 3 and have verified that these extra complications do not change in an important way, the qualitative features shown in Fig. 3 which was drawn from the evaluation of the simpler Eq. (11). The numerical differences between the two approaches agree to within a few percent at $T \approx 0K$ while at $T \approx 200K$ they differ at the 20% level. But this difference is not important for the conclusions we will make. What is critical is the sign of the Hall conductivity rather than its exact magnitude.

The boundary curves identified in Fig. 2 are reproduced on Fig. 3 as long dashed black lines. Our finite temperature data for the spin and valley Hall DC conductivity clearly reflects some of the features of these sharp crossovers but temperature does obscure their presence. Nevertheless our assignment of Chern numbers to various phases treating the gap as if it were effectively a zero temperature value, provides considerable insight into the origin of the complex variation of spin and valley Hall conductivity seen in Fig. 3. The left frames include the electron-phonon renormalization while the right frames do not and are for comparison. The top frames give the spin Hall and the lower frames give the valley Hall DC

conductivity. We first note that in our units, the spin Hall conductivity at $T=0$ is quantized and takes on the value zero for the larger values of $|\Delta_z|$ and $-1/\pi$ in the region of smaller $|\Delta_z|$. With a discontinuous crossover at $\tilde{\Delta}_{s_z}^\tau = 0$. Similarly the valley Hall conductivity jumps from $1/\pi$ to 0 and to $-1/\pi$ from right to left with boundaries also at $\tilde{\Delta}_{s_z}^\tau = 0$. As temperature is increased slightly the left (with electron-phonon) and right (without electron-phonon) panels remain practically indistinguishable. The crossover is no longer a jump but occurs over a small region of variation in Δ_z . However, at higher temperatures they become radically different. Without electron-phonon renormalization the sign of the spin Hall conductivity remains unchanged, while there can be sign changes when it is included. The region of small Δ_z is particularly interesting as we go from a topological insulator with effective Chern spin Hall number -1 to +1 by increasing T . The spin Hall conductivity goes from a negative at $T = 0K$ to a positive value at $T = 250K$ and this change in sign is taken as an indication of a topological crossover. It occurs only when the zero frequency value of the gap $\tilde{\Delta}_{s_z}^\tau$ changes sign with increasing T . This can never occur in a bare band picture and is a result of the electron-phonon renormalizations which become larger with increasing temperature and have the opposite sign to the bare gap $\Delta_{s_z}^\tau = \Delta_z - \lambda_{SO}\tau s_z$. Note that for a given valley the renormalized gap must be positive for one spin state and negative for the other so that both contributions add in the definition of the spin Hall conductivity to give a non zero value. Without a sign change the two contributions would cancel leading to zero spin Hall (trivial band insulator case).

In Fig. 4 we present results for the transverse AC conductivity based on Eq. (9) with matrix spectral density \tilde{A} obtained from the fully interacting Green's function specified in Eq. (5) to (7). The left frame gives the imaginary part of $\sigma_{xy}(\omega)$ in units of e^2/\hbar while the right gives the real part of the spin Hall $\sigma_{xy}^s(\omega)$. Top to bottom frames give three temperatures $T = 10K$ (top), $T = 160K$ (middle) and $T = 250K$ (bottom). In all cases the red curves are based on the bare bands for which Eq. (9) simplifies to Eq. (11). These are included for comparison with the dotted curves which fully include the electron-phonon renormalizations through the self energies $\Sigma^I(i\omega_n)$ and $\Sigma^Z(i\omega_n)$ of Eq. (3). Considering first the imaginary part $Im\sigma_{xy}(\omega)$ (left frames) we note that at low temperature $T = 10K$ bare (solid) and renormalized (dotted) results are not qualitatively different from each other. This is not the case at high temperatures. In particular for $T = 160K$ the sign associated with red ($\tau s_z = -1$) and black ($\tau s_z = +1$) curves is no longer the same. This arises because the sign of the renormalized results has reversed while that of the bare band results is unaltered. This shows once more how phonons can introduce temperature variation in the conductivity not part of bare band calculations. For $T = 250K$ the situation is even more complex with renormalized conductivity crossing at $\hbar\omega = 30meV$ (dotted curves). Turning next to the real

part of the spin Hall conductivity ($Re\sigma_{xy}^s(\omega)$) shown on the right in Fig. 4 we note again that renormalized (dotted) and bare band (solid) results agree qualitatively at low T but that this changes as T increases. Particularly important for this paper is the $\omega = 0$ limit which gives the DC value of the Hall conductivity used in Fig. 3. At low temperature bare and renormalized value agree while at higher T they in fact carry opposite sign as has been emphasized in constructing the color plots of Fig. 3.

IV. CIRCULAR POLARIZATION AND DICHOISM

Another consequence of the phonon renormalization of the effective gap is the change it can induce in the valley Hall optical selection rule for circularly polarized light. In Fig. 5 we show results for the frequency dependence of $Re\sigma_\pm(\omega)$ vs. ω in units of $\frac{e^2}{\hbar}$ at $T = 30K$ (upper panel) and at $T = 300K$ (lower panel). The solid red curve is $Re\sigma_+(\omega)$ for the spin up band and the red dotted is for spin down. Both show significant absorption above the main absorption edge determined by the effective low temperature gap. By contrast the black curves give $Re\sigma_-(\omega)$ and show that for this valley $\tau = 1$, there is comparatively little absorption of the left handed polarized light. This selection rule can be reversed by increasing temperature through a change in the sign of the effective gap brought about by the coupling to phonons as seen in the lower frame for $T = 300K$. This temperature is sufficiently large and the gap small enough that no absorption threshold can now be seen but it is clear that the left handed light is now more strongly absorbed than the right handed light. Finally we note sharp phonon structures at energies $(2|\Delta_{s_z}^\tau| + 2\omega_E)$ at low temperature. Of course once the sum over the two valleys $\tau = \pm 1$ is carried out these effects average out. However including a valley symmetry breaking term to our Hamiltonian (1) would allow the effect to be seen directly in optics.

V. CONCLUSION

Coupling of Dirac fermions to a phonon field can change the sign of their effective gap with increasing temperature. This leads to a rich set of crossovers from topological to band insulators with recognizable imprints in their DC spin Hall and valley Hall conductivity. It also leads to a switch with increasing temperature in the polarization from right to left handedness of the dominantly absorbed light by a given valley. Both effects provide a pathway to the experimental verification of such a phonon induced topological crossover.

ACKNOWLEDGMENTS

This work was supported by the Natural Sciences and Engineering Research Council of Canada (NSERC), the Canadian Institute for Advanced Research (CIFAR).

REFERENCES

-
- * lizhou@mcmaster.ca
- ¹ K. S. Novoselov, D. Jiang, F. Schedin, T. J. Booth, V. V. Khotkevich, S. V. Morozov, and A. K. Geim, *Proc. Natl. Acad. Sci. USA* **102**, 10451(2005).
 - ² K. S. Novoselov, A. K. Geim, S. V. Morozov, D. Jiang, Y. Zhang, S. V. Dubonos, I. V. Grigorieva and A. A. Firsov, *Science* **306**, 666 (2004).
 - ³ X. Zhang, Y.-W. Tan, H. L. Stormer and P. Kim, *Nature* **438**, 201 (2005).
 - ⁴ A. K. Geim and K. S. Novoselov, *Nat. Mater.* **6**, 183 (2007).
 - ⁵ T. Cheiwchanchamnangij and W. R. L. Lambrecht, *Phys. Rev. B* **85**, 205302 (2012).
 - ⁶ Z. Y. Zhu, Y. C. Cheng and U. Schwingenschlögl, *Phys. Rev. B* **84**, 153402 (2011).
 - ⁷ W. Feng, Y. Yao, W. Zhu, J. Zhou, W. Yao and D. Xiao, *Phys. Rev. B* **86**, 165108 (2012).
 - ⁸ Zhou Li and J. P. Carbotte, *Phys. Rev. B* **86**, 205425 (2012).
 - ⁹ B. Aufray, A. Kara, S. Vizzini, H. Oughaddou, C. Léandri, B. Ealet and G. Lay, *Appl. Phys. Lett.* **96**, 183102(2010).
 - ¹⁰ P. De Padova, C. Quaresima, C. Ottaviani, P. M. Sheverdyaeva, P. Moras, C. Carbone, D. Topwal, B. Olivieri, A. Kara, H. Oughaddou, B. Aufray, and G. Lay, *Appl. Phys. Lett.* **96**, 261905 (2010).
 - ¹¹ L. Stille, C. J. Tabert and E. J. Nicol, *Phys. Rev. B* **86**, 195405 (2012).
 - ¹² C. L. Kane and E. J. Mele, *Phys. Rev. Lett.* **95**, 226801 (2005).
 - ¹³ D. Xiao, W. Yao and Q. Niu, *Phys. Rev. Lett.* **99**, 236809 (2007).
 - ¹⁴ D. Xiao, G. B. Liu, W. Feng, X. Xu and W. Yao, *Phys. Rev. Lett.* **108**, 196802 (2012).
 - ¹⁵ H. Zeng, J. Dai, W. Yao, D. Xiao and X. Cui, *Nature Nano.* **7**, 490 (2012).
 - ¹⁶ K. F. Mak, K. He, J. Shan and T. F. Heinz, *Nature Nano.* **7**, 494 (2012).
 - ¹⁷ T. Cao, G. Wang, W. Han, H. Ye, C. Zhu, J. Shi, Q. Niu, P. Tan, E. Wang, B. Liu and J. Feng, *Nature Communications.* **3**, 887 (2012).
 - ¹⁸ Zhou Li and J. P. Carbotte, *Physica B* **421**, 97 (2013), DOI: 10.1016/j.physb.2013.04.030.
 - ¹⁹ J. P. Carbotte, E. J. Nicol and S. G. Sharapov, *Phys. Rev. B* **81**, 045419 (2010).
 - ²⁰ T. Stauber and N. M. R. Peres, *J. Phys.: Condens. Matter* **20**, 055002 (2008).
 - ²¹ A. Pound, J. P. Carbotte and E. J. Nicol, *Phys. Rev. B* **85**, 125422 (2012).
 - ²² Ion Garate, *Phys. Rev. Lett.* **110**, 046402 (2013).
 - ²³ Takeshi Kondo, Y. Nakashima, Y. Ota, Y. Ishida, W. Malaeb, K. Okazaki, S. Shin, M. Kriener, Satoshi Sasaki, Kouji Segawa, and Yoichi Ando, *Phys. Rev. Lett.* **110**, 217601 (2013).
 - ²⁴ R. C. Hatch, D. L. Huber and H. Höchst, *Phys. Rev. Lett.* **104**, 047601 (2010).
 - ²⁵ E. Cappelluti and L. Benfatto, *Phys. Rev. B* **79**, 035419 (2009).
 - ²⁶ L. Benfatto, S. G. Sharapov, N. Andrenacci and H. Beck, *Phys. Rev. B* **71**, 104511 (2005).